EXAFS and XANES Study of a Pure and Pd Doped Novel Sn/SnO_x Nanomaterial

Didier Grandjean*

Department of Inorganic Chemistry and Catalysis, Debye Institute, Utrecht University, Sorbonnelaan 16, 3584 CA Utrecht, The Netherlands

Robert E. Benfield

Functional Materials Group, School of Physical Sciences, University of Kent, Canterbury CT2 7NR, U.K.

Céline Nayral, André Maisonnat, and Bruno Chaudret

Laboratoire de Chimie de Coordination CNRS, 205, route de Narbonne, 31077 Toulouse, Cedex 04, France

Received: October 10, 2003; In Final Form: April 6, 2004

EXAFS and XANES at the Pd and/or Sn K-edge have been used to characterize pure and palladium doped spherical particles (10−63 nm diameter) of a novel Sn/SnO_x nanocomposite. This nanomaterial prepared by decomposition of organic precursors has found application in a new type of high performance solid-state gas sensor. Except for the sample annealed at 600 °C that is mainly pure crystalline tetragonal cassiterite SnO_2, the undoped nanoparticles consist of a Sn metallic core surrounded by a layer of tin oxide that is mostly amorphous. In this outer layer, tin atoms were found to be 4−5-fold coordinated to oxygen with bond distances slightly larger than in bulk cassiterite SnO_2. The average tin oxidation state in the oxide phase was evaluated using the length of the tin−oxygen bond to be between +3.7 and +3.5. The relative ratio of Sn atoms in the metallic phase was estimated between 15 and 36% of the total number of Sn atoms using the coordination number of the first Sn shell corresponding to the tin β tetragonal metallic phase. In the palladium doped samples prepared either by codecomposition of Sn and Pd organometallic precursors (volume-doped) or by deposition of palladium on preformed Sn/SnO_x nanoparticles (surface-doped) palladium was found surprisingly to be always in a metallic state, and no trace of oxidation of the Pd atoms could be detected. In both samples Pd is surrounded by ca. 2.6 Sn at unusually short distances varying from 2.55 Å in the volume-doped sample to 2.58 Å in the surface-doped sample and by a second coordination shell of ca. 2.3 Pd atoms located at 2.77 Å in the Pd surface-doped sample and only 0.5 Pd atoms in the Pd volume-doped sample. These results show that the volume doping method leads to a more homogeneous mixing of the Pd atoms in the Sn matrix since much fewer Pd atoms were found in the Pd coordination shell. This is consistent both with the large increase in the particle diameter observed by HRTEM and the poor electrical properties that have been measured for the fully oxidized Pd volume-doped materials. In combination with HRTEM, two structural models for the doped materials are discussed: formation of small metallic Pd platelets around the tin metallic core by complex migration and rearrangement of the Pd atoms and/or formation of a new mixed Pd/Sn phase in the metallic core of the particle.

1. Introduction

In the field of solid-state gas sensors the trend to use integrated circuit technology to produce low cost, high reliability silicon platform for SnO_2-based sensors is developing very rapidly. At the same time several studies have shown that reducing the crystallite size of the active tin oxide material results in a big improvement in its sensing properties and stability over time. Several preparation methods such as sputtering either from a tin oxide[1] or a tin metal target,[2] chemical vapor deposition,[3] or sol−gel processes[4−7] are commonly employed to produce a nanocrystalline SnO_2 material. However these techniques generally suffer from a poor control of the grain morphology and lead to a material with a low specific surface that presents a drift of its conductance properties over time.

In an attempt to overcome these problems, we have developed a new chemical method based on the decomposition of the organometallic precursor $[Sn(NMe_2)_2]_2$ in a controlled water/anisole mixture that leads to the formation of a suspension of monodisperse nanocomposites of Sn/SnO_x in a colloidal solution.[8−10] These nanoparticles are of very small size (ca. 12 nm in average) and tend to form agglomerates. To increase the dispersion of the particles, the decomposition of the organometallic precursor can be carried out in the presence of a poly (N-vinyl pyrolid-2-one) (pvp) polymer to obtain Sn/SnO_x colloids coated with polymer. A subsequent heat treatment of these colloids, coated or not with the pvp polymer, carried out at 600 °C leads in all cases to SnO_2 nanoparticles that retain the same size and morphology.

A new operational high performance gas sensor has been designed by depositing a drop of a suspension of these nanocomposite particles onto a silicon die. This drop is then heated to 525 °C using the integrated heater, and a thin film of highly sensitive SnO_2 nanoparticles is generated onto the surface of the silicon wafer.[11,12]

* To whom correspondence should be addressed. Fax: + 3130 251 1027. E-mail: D.Grandjean@chem.uu.nl.

10.1021/jp0370627 CCC: $27.50 © 2004 American Chemical Society
Published on Web 06/09/2004

Another way to improve the performance of these SnO_2-based sensors both in term of sensitivity and response time for a broad range of gases is doping them with small amounts of a noble metal like palladium.[13−16] In this case, the sensitivity and selectivity properties have been shown to depend greatly both on the crystal size and the distribution of the added noble metals.[17−20] To achieve an homogeneous Pd doped SnO_2 sensor layer starting from our nanocomposite material, two different routes have been investigated: codecomposition of Sn-based and Pd-based organometallic precursors (doping in volume) and deposition of palladium on preformed Sn/SnO_x nanoparticles (doping in surface). Doping in surface lead to a big improvement of the conducting properties of the fully oxidized material but the codecomposition route (doping in volume) gave a material with poorer conducting properties than the undoped one.

These contradictory results show that the location of the dopants atoms may be more complex than a surface or volume doping that has been simplistically assumed so far. A detailed investigation of the morphology, the structure, and the electronic properties of both pure and Pd doped precursor Sn/SnO_x nanocomposites in solution as well as in the heat-treated SnO_2 material is crucial to achieve full control and understanding of the relationship between the structure of these materials and their properties. A great variety of techniques such as Mössbauer spectroscopy, XPS, HRTEM, and X-ray diffraction have already been used to characterize these new nanomaterials; however, they have all shown some limitations relative to the complex nature of these systems. For instance, the use of techniques such as X-ray diffraction to study this type of nanomaterials can sometimes be misleading since it is only sensitive to ordered structures. Electron microscopy can achieve direct imaging of the particles, but this method covers only local areas of the sample, which may not be representative of the whole material. At the same time some amorphous part of the sample may be difficult to interpret or simply to image. XPS is a reliable technique to determine the oxidation state of the different atoms present in the material but is very surface sensitive. Moreover our XPS measurements showed a Pd $3d_{5/2}$ peak located at 335.8 eV in the Pd doped Sn/SnO_x composite which is a value too close in energy to those reported both for Pd^0 and PdO[21] to allow for an accurate determination of the palladium oxidation state by this method. Crucial information such as the bulk oxidation state of both Sn and Pd atoms and the local structure around both atoms in the amorphous domains as well as the location of the Pd dopant in the materials are indeed difficult to obtain using these techniques alone.

An X-ray absorption spectroscopy (XAS) technique that does not rely on long-range order is particularly well suited to characterize the geometrical structures and bond distances in materials that lack detectable long-range order such as the Sn/SnO_x nanocomposites as well as to give insight into their electronic structure. Another advantage of the XAS technique is that it is element specific and thus can allow for the local order around Sn and Pd to be investigated independently. For these reasons, these techniques have already been extensively applied to characterize several types of fully oxidized pure or doped SnO_2 nanomaterials,[22−36] and important information such as the nanocrystallite sizes as well as the location of the dopant atom could be successfully unravelled. If a large variety of dopant atoms has been investigated by XAS in this system, except for an EXAFS study on an alumina-supported Pd catalyst modified with tin atoms[37] and a preliminary work carried out on Sn−Pd bimetallic colloids,[38] no extensive study using this technique has been reported on Pd doped SnO_2 materials.

We report here an EXAFS and XANES study at the Pd and/or Sn K-edges in pure Sn/SnO_x colloidal suspension coated or not with pvp and after heat-treatment as well as in two Pd doped Sn/SnO_x samples prepared by two different methods. The aims of this study are to complement the characterization methods already used by a local order sensitive probe to better characterize the local structure and the electronic properties as well as to determine the dopant location in these novel Sn/SnO_x colloidal suspensions, precursors of the SnO_2-based sensor nanomaterials. Both a better understanding and monitoring of the synthesis process are essential in order to develop a reproducible low-cost synthetic method for a large-scale production of these new types of gas sensors.

2. Experimental Section

2.1. Preparation of the Nanocomposites. *2.1.1. Materials and Reagents.* All compounds used in this work were sensitive to oxygen and moisture and were manipulated in a standard vacuum line or in argon atmosphere by using an MBraun Inert Gas System. The preparation of the tin colloid and the palladium precursors ($[Pd(dba)_2]$) follows the routes described earlier.[39] Anisole was purchased from Aldrich, and its water content was checked by Karl-Fisher coulometric titration by using Metrohm equipment.

2.1.2. Preparation of the $[Sn/SnO_x]$ Colloidal Suspension. Preparation of the tin colloid follows the route described previously.[10,11] The precursor $[Sn(NMe_2)_2]_2$ (174 mg, 0.42 mmol; 0.84 10−3 eq Sn) in anisole (degassed under vacuum, at liquid nitrogen temperature; 15 mL) containing traces of water (0.4 mg/mL of anisole; 0.33 mmol: $[H_2O]/[Sn] = 0.4$) was heated at 135 °C under magnetic stirring in a Fischer−Porter bottle. The initial yellow solution darkened within 10 min and a black solid progressively precipitated. After 3 h, the solution was removed by filtration, and the black precipitate was washed with anisole (3×40 mL). The black solid was then redispersed in 15 mL of degassed anisole, and the Fischer−Porter bottle was pressurized to 3 bars of dihydrogen. After stirring for 3 h, the resulting suspension was sampled for TEM analysis that showed the presence of nanoparticles of 7−20 nm diameter (Gaussian fit, mean size: 13.2 (2.2) nm).

2.1.3. Preparation of $[Sn/SnO_x]$ Colloids Embedded in a pvp Polymer Matrix. Tin colloids embedded in a pvp matrix were prepared by adding poly (N-vinyl pyrolid-2-one) (pvp) to the previous reactional mixture in a ratio of $[Sn]/[pvp] = 50$ wt %. As previously, the solution darkened after a 3-h heat treatment at 135 °C, and a black solid progressively precipitated. TEM analysis showed the presence of chains of particles, of similar sizes to those of the colloids obtained without polymer, relatively well dispersed into the pvp matrix.

2.1.4. Preparation of Pd Doped in Surface $[Sn/SnO_x]$ Colloidal Suspension. A palladium precursor (4.8 mL of a solution containing 20.0 mg of $[Pd(dba)_2]$ in 10 mL of anisole was added to a colloidal suspension of $[Sn/SnO_x]$ in anisole (0.42 10^{-3} eq Sn; 15 mL); 0.0167 mmol; $[Pd]/[Sn] = 4$ wt %). After exposition to 1 bar of CO during 20 min, depressurization, sampling for TEM, HRTEM, EDX, and XPS experiments, decantation filtration, and drying under vacuum, a black powder was obtained. Elemental analysis gave 73.72% of Sn and 2.06% of Pd; $[Pd]/[Sn] = 3.09$ wt % (doping yield: 77%). TEM analysis showed the presence of nanoparticles of 7−19 nm diameter (Gaussian fit, mean size: 13.2 (1.7) nm).

2.1.5. Preparation of Pd Doped in Volume $[Sn/SnO_x]$ Colloidal Suspension. The palladium precursor $Pd(OAc)_2$ was added to a solution of $[Sn(NMe_2)_2]_2$ in anisole (degassed under

vacuum, at liquid nitrogen temperature; 15 mL) containing traces of water (0.2 mg/mL of anisole; 0.33 mmol: $[H_2O]/[Sn] = 0.2$) in a [Pd]/[Sn] ratio of 8 wt %. The solution was then heated at 135 °C for 3 h under magnetic stirring, and a black suspension was obtained. After decantation the black precipitate was washed with anisole (3×40 mL). TEM analysis showed large spherical nanoparticles of ca. 63 nm diameter, while EDX analysis confirmed the presence of Pd in the sample.

2.1.6. Thermal Oxidation of Pure Sn/SnO$_x$ Nanocomposites. The black solids resulting from the decomposition of $[Sn(NMe_2)_2]_2$ in anisole were heat-treated in air in an oven for a period of 135 min at temperatures ranging from 50 to 600 °C according to the optimized multistep process that has been described previously.[9]

2.1.7. Electron Microscopy Experiments. Samples for TEM studies were prepared in a glovebox by slow evaporation of a drop of suitably diluted colloidal suspensions deposited on holey carbon-covered grids. The TEM experiments were performed at the "Service Commun de Microscopies de l'Université Paul Sabatier" on a JEOL JEM 200CXT-T electron microscope working at 200 kV and a Philips CM12 electron microscope working at 120 kV, while the high-resolution images were obtained with a JEOL JEM 2010 electron microscope operating at 200 kV. The size distribution of the particles was determined from enlarged photographs by measuring a minimum of 200 particles for each example.

2.2. X-ray Absorption Spectroscopy. X-ray absorption data were collected on beamline 9.2 (CLRC Daresbury Laboratory, U.K.), operating under beam conditions of 2 GeV, 200 mA using a Si (220) double-crystal monochromator. The monochromator was detuned on its rocking curve to approximately 60% of the maximum transmitted X-ray intensity to reduce the harmonic content of the beam at a minimum level. Appropriate amounts of sample were finely ground with boron nitride and pressed (5 bar) into 13 mm pellets producing a suitable edge jump. The spectra were recorded at 80 K by cooling the samples with a coldfinger liquid-nitrogen cryostat. XAS signals were measured in transmission mode at the Sn K edge (29200.1 eV) and in fluorescence mode using a 13-channel solid-state detector at the Pd K edge (24350.3 eV) with, in most of the cases, several data sets summed to improve signal/noise ratios. For the measurements at Pd K-edge only one EXAFS spectrum was collected for each sample. Cassiterite SnO_2 and PdO powder (Aldrich 99.999%) that were used as reference samples were also studied in transmission. Ionization chambers were filled with standard Ar/Kr mixtures. Exact calibration of the X-ray energy for detailed comparison of the XANES features was achieved by simultaneously recording a Sn or Pd foil spectrum in the monitor position using a third ionization chamber. Data were collected with acquisition times up to 35 min (1−6 s acquisition time/point).

Data reduction of experimental X-ray absorption spectra was performed using the program EXBROOK.[40] Preedge background subtraction and normalization was carried out by fitting a linear polynomial to the preedge region and cubic splines to the postedge region of the absorption spectrum. A smooth atomic background was then obtained. To obtain a reliable alignment of the XANES spectra, the first derivatives of the raw data from the monitor channel were linearly calibrated and superimposed on each other. EXAFS refinements were performed with the EXCURV98 package.[40] Phase shifts and backscattering factors were calculated ab initio using Hedin-Lundqvist potentials. Refinements were carried out using k^3 weighting for the reference compounds and k^2 for all the other ones in the range 2.5−3 to 12−15 Å^{-1}. To improve the quality of the signal for a better quantitative analysis and to reduce the number of fitting parameters, the data for all the samples (except for bulk Sn and Pd) were refined using Fourier filtering techniques. To minimize systematic errors that might arise from cutoff effects, the same filter window (0.8−4.0 Å) was applied to all samples. Fourier transforms (FT's) peaks were isolated with a Gaussian window, and the contribution of these groups of shells was extracted by inverse transformation.

3. Results and Discussion

3.1. Electron Microscopy HRTEM. Figure 1a shows the HRTEM image of a typical composite pure tin nanoparticle in colloidal suspension[8,9] that is clearly composed of a crystallized core of ca. 12 nm diameter surrounded by an amorphous layer of ca. 4 nm. The results of the XRD and Mössbauer analyses[9] are consistent with the presence of an amorphous tin oxide surface layer surrounding a β crystallized tin core. However the exact coordination and oxidation state of tin in this outer layer could not be unravelled. Figure 1b shows the HRTEM image of a typical Sn/SnO$_x$ nanoparticle surface-doped with Pd. The particles retain the same size as in the pure Sn/SnO$_x$ nanocomposite and the same basic appearance, but the core part appears to be surrounded by some small platelets of well-crystallized materials. Figure 1c displays a typical palladium volume doped tin particle. It is obvious that the particle size has increased dramatically to reach ca. 63 nm in diameter. As in the case of surface doped particles, the core of the particle appears to be surrounded by platelets of a rather crystalline material embedded in an outer amorphous layer. The complexity of these systems shows that numerous important points such as the nature of the amorphous phase as well as the composition of the platelets appearing around the amorphous layer in the Pd doped tin material remain unclear. To complement the HRTEM results and obtain information on the exact location and the coordination of the dopant atoms, the use of a technique sensitive to the local order around a specific atom such as the X-ray absorption spectroscopy technique is necessary.

3.2. XANES. XANES that corresponds to an electronic transition from inner electronic levels to outer unoccupied levels gives useful structural information such as oxidation state of chemical species, site symmetry, and covalent bond strength and has widely been used to infer the local structure around the central atom. Background corrected and normalized experimental XANES Sn K-edge and Pd K-edge spectra are respectively shown in Figures 2 and 3. The absorption edge maximum represents in this case an allowed 1s−5p transition that merges into the continuum at higher energies.

3.2.1. Sn K-Edge. Figure 2 shows that except for the sample oxidized at 600 °C, all the Sn/SnO$_x$ nanomaterials present a very similar XANES profile. They all feature the white line characteristic of the oxide species but with a lower intensity than for the SnO_2 reference compound. The lower intensity of the white line shows that the average oxidation state of Sn in this material is lower than that in the bulk SnO_2 (+IV) material. Compared with the bulk SnO_2 reference compound, the Sn/SnO$_x$ nanocomposites XANES spectra are also characterized by damped resonance peaks that usually shows the presence of a disordered and/or a large number of surface atoms. A mixture of an amorphous SnO_2 phase with a Sn metallic phase may be a possible explanation of the shape of this XANES profile.

The position of the edge that is usually taken as the maximum of the first derivative of the XANES spectra can also be used to evaluate the oxidation state of the absorbing atom: a shift

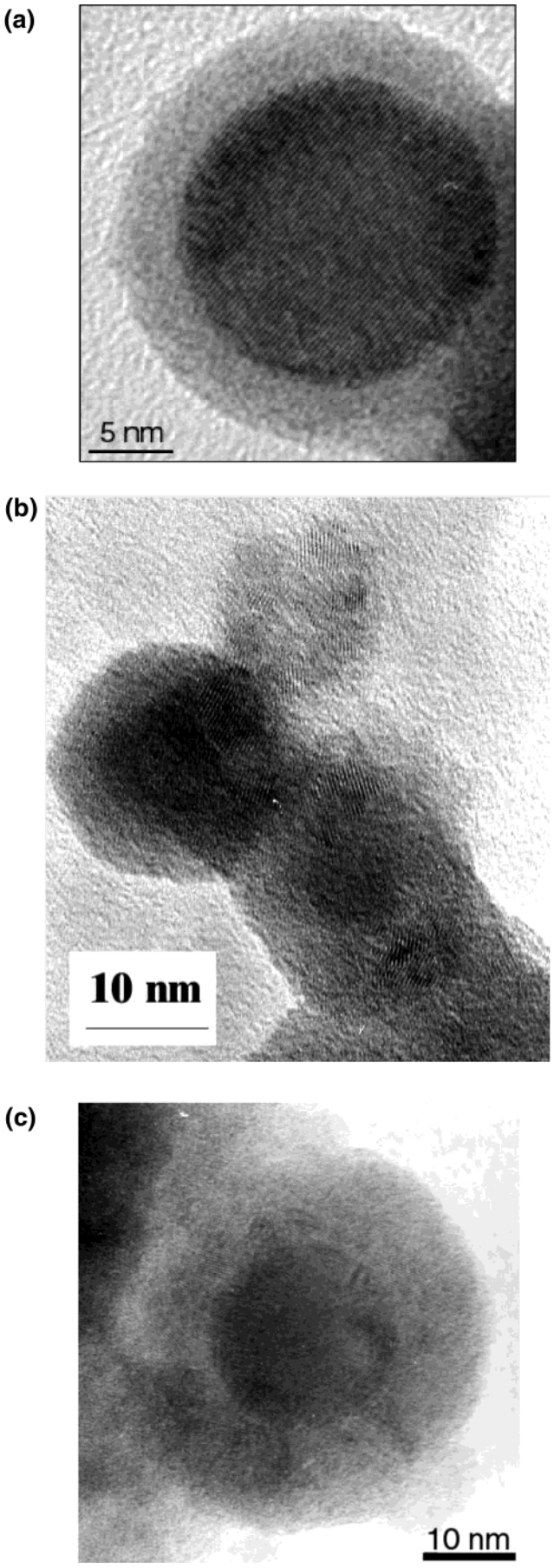

Figure 1. HREM images of **a**: a Sn/SnO_x nanoparticle; **b**: Sn/SnO_x nanoparticle surface-doped with Pd; **c**: Sn/SnO_x nanoparticle volume-doped with Pd.

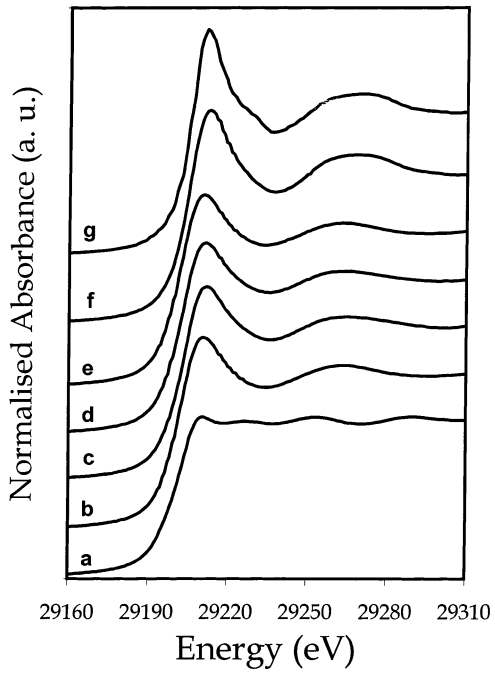

Figure 2. Sn K-edge normalized XANES spectra of the series of Sn/SnO_x nanomaterials and reference samples. **a**: bulk Sn; **b**: Sn/SnO_x; **c**: Sn/SnO_x surface-doped with Pd; **d**: Sn/SnO_x volume-doped with Pd; **e**: Sn/SnO_x coated in pvp; **f**: Sn/SnO_x annealed at 600 °C; **g**: bulk SnO_2.

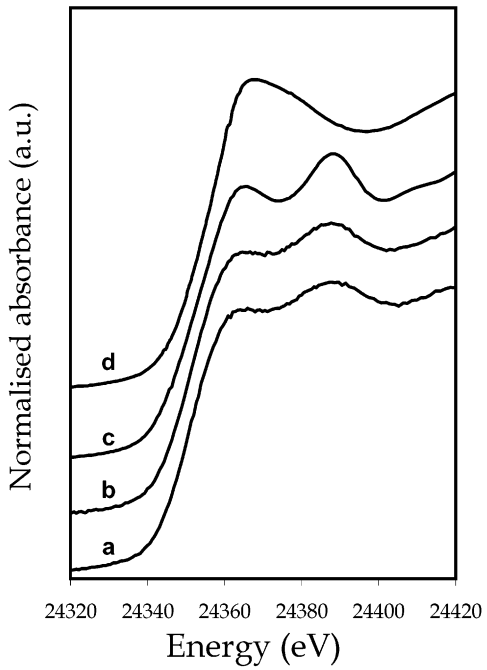

Figure 3. Pd K-edge normalized XANES of Pd doped Sn/SnO_x nanomaterials and reference samples. **a**: Sn/SnO_x volume-doped with Pd; **b**: Sn/SnO_x surface-doped with Pd; **c**: bulk Pd; **d**: bulk PdO.

toward higher energies is generally attributed to an increased oxidation state of the metal.[41,42] Compared to the reference sample SnO_2, that have an edge position located at 29 205.3 eV, the heat-treated Sn/SnO_x sample has an identical edge position indicating that tin in this material is likely to be fully oxidized into SnO_2. Moreover this sample features a very similar XANES profile to the bulk cassiterite SnO_2 both in terms of shape and location of the resonance peaks indicating a similar structure. However the intensity of the white line, slightly lower than in bulk SnO_2, may indicate the presence of some trace of

TABLE 1: Summary of Structural Results of Sn K-Edge EXAFS Refinements of Sn/SnO_x Nanomaterials along with Bulk Tin and Bulk Cassiterite SnO_2[a]

	bulk Sn	bulk SnO_2	Sn/SnO_x colloids	Sn/SnO_x in pvp	Pd volume-doped Sn/SnO_x	Pd surface-doped Sn/SnO_x	heat-treated 600 °C Sn/SnO_x
E_f (eV)	−6.1 (5)	−4.8 (7)	−8.8 (5)	−9.3 (4)	−8.5 (3)	−6.8 (5)	−7.3 (5)
AFAC	1	1	1	1	1	1	1
k	3	3	2	2	2	2	3
k-range	3−14	3−15	2.5−15	2.5−15	2.5−15	2.5−15	3−15
N_1	4[b] Sn	6[b] O	3.3 (2) O	3.2 (1) O	3.3 (1) O	3.3 (2) O	6[b] O
R_1	3.001 (2)	2.041 (4)	2.074 (5)	2.091 (4)	2.071 (4)	2.073 (4)	2.058 (5)
A_1	0.016 (1)	0.007 (1)	0.010 (1)	0.009 (1)	0.010(1)	0.008 (1)	0.006 (1)
N_2	4[b] Sn	2[b] Sn	1.4 (5) Sn	0.6 (4) Sn	0.9 (3) Sn	1.1 (4) Sn	2[b] Sn
R_2	3.705 (3)	3.200 (5)	3.01 (2)	2.98 (2)	3.00 (1)	3.01 (1)	3.200 (5)
A_2	0.050 (1)	0.009 (1)	0.021 (7)	0.014 (6)	0.014 (5)	0.010 (4)	0.003 (1)
N_3		4[b] O	0.6 (3) Sn	1.0 (9) Sn	0.8 (3) Sn	1.9 (7) Sn	4[b] O
R_3		3.63 (2)	3.250 (7)	3.34 (4)	3.25 (1)	3.27 (2)	3.61 (3)
A_3		0.002 (4)	0.005 (3)	0.03 (2)	0.010 (4)	0.021 (8)	0.006 (9)
N_4		8[b] Sn		0.3 (2) Sn		0.6 (5) Sn	8[b] Sn
R_4		3.704 (7)		3.75 (1)		3.75 (2)	3.720 (4)
A_4		0.014 (1)		0.001 (7)		0.009 (8)	0.006 (1)
N_5						0.1 (1) Pd	
R_5						2.58 (2)	
A_5						0.0006 (−)	
R (%)	14.7	19.4	18.4	18. 2	15.1	18.6	14.4

[a] E_f = contribution of the wave vector of the zero photoelectron relative to the origin of k [eV]. AFAC = amplitude reduction due to many-electron processes. N_i = number of atom in the ith shell. R_i = radial distance of atoms in the ith shell [Å]. A_i = Debye−Waller term of the ith shell ($A = 2\sigma^2$ with σ = Debye−Waller factor) [Å^2]. R factor in %. [b] These parameters were kept fixed during the refinement. Bulk Sn: $I41/amd$; $a = b = 5.831$ Å, $c = 3.182$ Å; 4Sn at 3.022 Å, 2Sn at 3.182 Å, 4Sn at 3.768 Å.[43] Bulk SnO_2: $P42/mnm$ cassiterite; $a = b = 4.737$ Å, $c = 3.185$ Å; 4O at 2.051 Å, 2O at 2.057 Å, 4O at 3.590 Å.[43] Bulk SnO: $P4/nmm$ romarchite $a = b = 3.796$ Å, $c = 4.816$ Å; 4O at 2.211 Å, 4Sn at 3.515 Å, 4Sn at 3.700 Å.[43]

another phase such as SnO or possibly some remaining metallic tin. The edge position for the other Sn/SnO_x nanocomposites was ranging from 29 201 eV in the sample coated with pvp, 29 203.1 eV in the Sn/SnO_x nanocomposite, to 29 203.8 eV in the Pd doped samples confirming the partial oxidation of the tin atoms. However, the determination of an edge position in a multiphasic material is difficult, and its translation into an average oxidation state often unreliable.

3.2.2. Pd K-Edge. Figure 3 presents the XANES of two Sn/SnO_x nanomaterials doped with Pd using two different preparation methods i.e., volume-doped and surface-doped along with bulk PdO and Pd metal presented as references. The two Pd doped Sn/SnO_x XANES spectra are almost identical except for a slight shift toward higher energies of the volume-doped spectrum relative to the surface-doped one. These two samples prepared using two different methods seem to have a very close average electronic structure. When compared to the spectrum of bulk palladium, the general profile of the two spectra corresponding to the Pd doped materials is very similar. However, the two main resonance features of Pd doped Sn/SnO_x are very much damped in comparison to the bulk metallic Pd indicating the presence of disorder in the material and/or nanosize structures. The PdO spectrum has a totally different shape and is obviously shifted toward the higher energies as one might expect it in the case of a higher oxidation state (+II). Indeed, the absorption edge for PdO is located at 24 360 eV compared with 24 350 eV for the bulk Pd and both Pd doped Sn/SnO_x samples. The XANES analysis can already show that the Pd in the doped Sn/SnO_x samples is not oxidized and has an electronic structure close to the metallic state but with very small particle size and/or amorphous character. The slight shift observed between the two spectra suggests that Pd features a slightly different environment in each doped sample.

3.3. EXAFS. Results of the EXAFS structural refinements are summarized in Table 1 for the Sn K-edge measurements and in Table 2 for the Pd K-edge measurements. All the EXAFS best fits with R-factors in the range of 14.3−19.4% for Sn and Pd K edges are presented respectively in Figures 4 and 5. The Fourier transform best fits for Sn and Pd K-edges are presented in Figures 6 and 7, respectively.

TABLE 2: Summary of Structural Results of Pd K-Edge EXAFS Refinements of the Pd Doped Sn/SnO_x Nanomaterials along with Bulk Pd and Bulk PdO[a]

	bulk Pd	PdO	Pd volume-doped Sn/SnO_x	Pd surface-doped Sn/SnO_x
E_f (eV)	−0.4(2)	4.7 (7)	−4.0 (8)	−4.6 (4)
AFAC	0.80	0.80	0.80	0.80
k	3	3	2	2
k-range	3−16	3−15	3−14	3−14.5
N_1	12[b] Pd	4[b] O	2.6 (5) Sn	2.8 (4) Sn
R_1	2.737 (1)	2.005 (1)	2.55 (1)	2.58 (1)
A_1	0.0100 (1)	0.003 (1)	0.005 (1)	0.012 (1)
N_2	6[b] Pd	4[b] Pd	0.5 (4) Pd	2.3 (6) Pd
R_2	3.87 (1)	3.030 (2)	2.71 (4)	2.77 (1)
A_2	0.018 (4)	0.004 (1)	0.001 (2)	0.012 (3)
N_3	24[b] Pd	8[b] Pd		
R_3	4.741 (6)	3.416 (4)		
A_3	0.016 (2)	0.005 (1)		
N_4	12[b] Pd			
R_4	5.47 (2)			
A_4	0.023 (3)			
N_5	24 Pd			
R_5	6.13 (3)			
A_5	0.028 (1)			
R (%)	15.3	17.7	16.4	14.3

[a] E_f = contribution of the wave vector of the zero photoelectron relative to the origin of k [eV]. AFAC = amplitude reduction due to many-electron processes. N_i = number of atom in the ith shell. R_i = radial distance of atoms in the ith shell [Å]. A_i = Debye−Waller term of the ith shell ($A = 2\sigma^2$ with σ = Debye−Waller factor) [Å^2]. R factor in %. [b] These parameters were kept fixed during the refinement. Bulk Pd: fcc $a = 3.8898$ Å, 12Pd at 2.751 Å, 6Pd at 3.890 Å.[43] Bulk PdO: $P42/mmc$ $a = b = 3.03$ Å, $c = 5.33$ Å 4O at 2.018 Å, 2Pd at 2.665 Å, 4Pd at 3.030 Å.[43]

3.3.1. Sn K-Edge. The phase corrected FT's of all the samples under investigation at the Sn K edge are gathered in Figure 8. Before phase correction, they all present a first neighbor peak

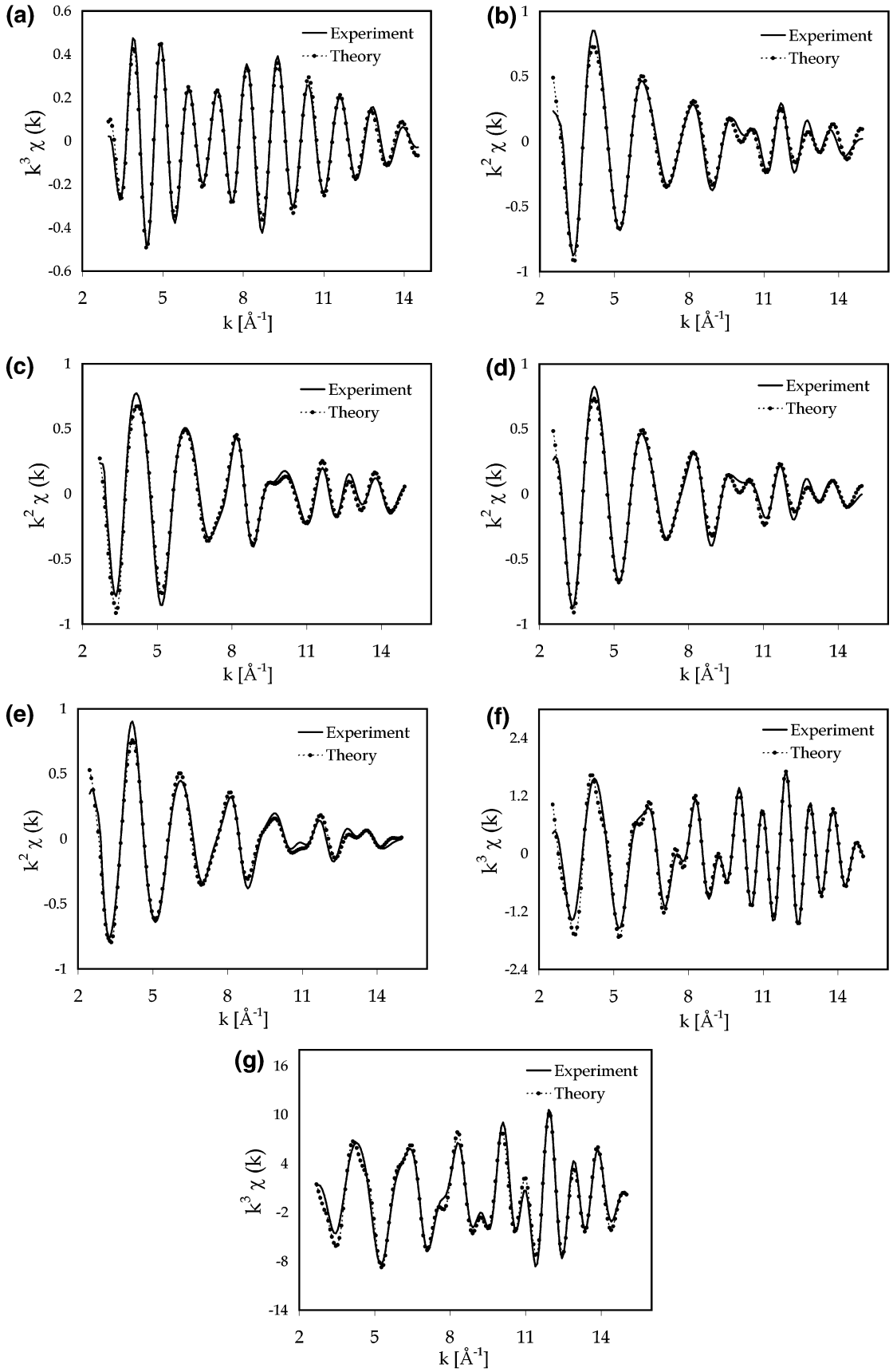

Figure 4. Sn K-edge EXAFS spectra (after background subtraction, k^3-weighted or k^2-weighted) of the series of Sn/SnO$_x$ nanomaterials and reference samples. **a**: bulk Sn; **b**: Sn/SnO$_x$; **c**: Sn/SnO$_x$ surface-doped with Pd; **d**: Sn/SnO$_x$ volume-doped with Pd; **e**: Sn/SnO$_x$ coated in pvp; **f**: Sn/SnO$_x$ annealed at 600 °C; **g**: bulk SnO$_2$. The solid lines are the experimental data, and the dotted lines are the best fit.

located at a distance of ca. 1.7 Å corresponding to an oxygen shell. As far as the higher distance shells are concerned there is a great variety of cases when going from Sn/SnO$_x$ colloids coated with pvp polymer in which only very small peaks are

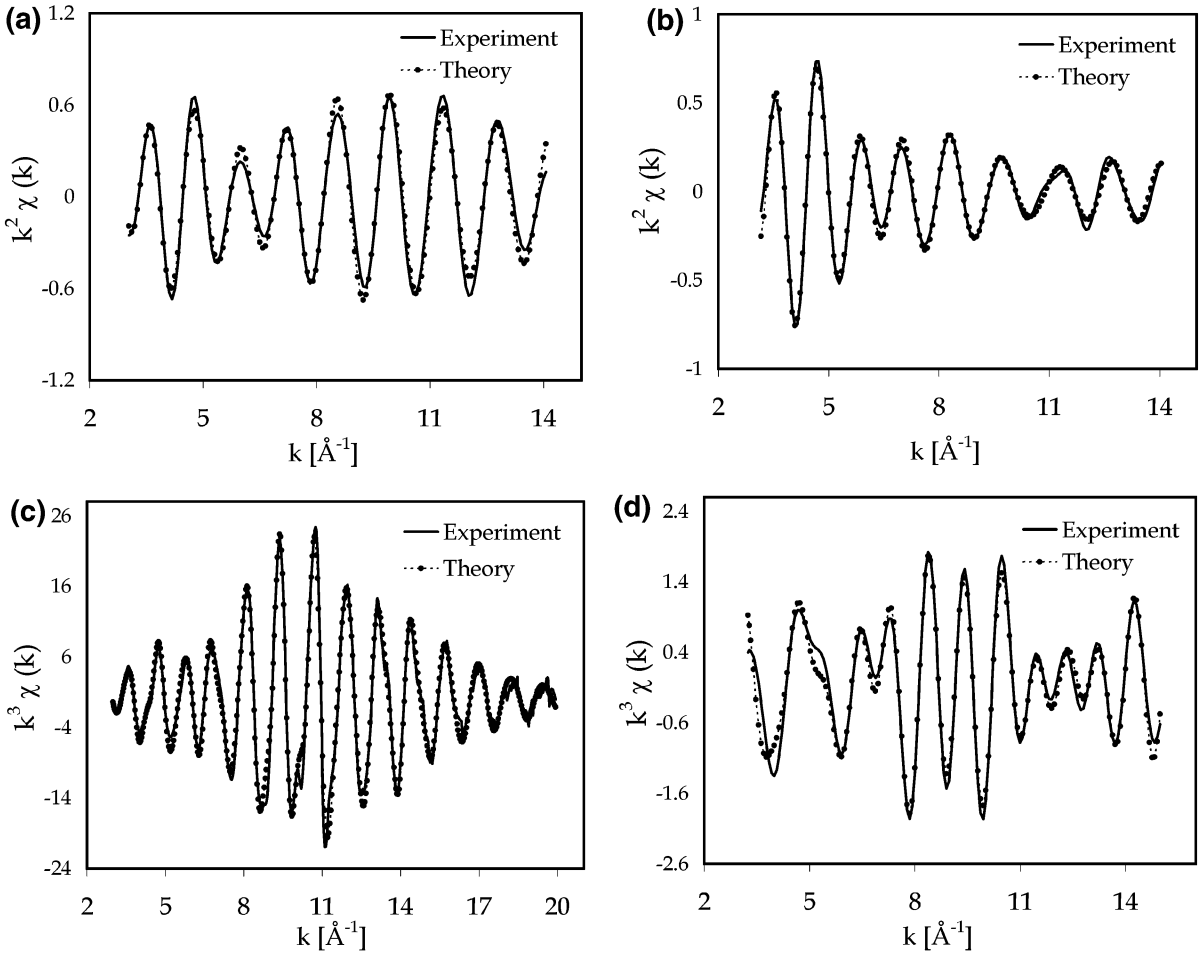

Figure 5. Pd K-edge EXAFS spectra (after background subtraction, k^3-weighted or k^2-weighted) of Pd doped Sn/SnO_x nanomaterials and reference samples. **a**: Sn/SnO_x volume-doped with Pd; **b**: Sn/SnO_x surface-doped with Pd; **c**: bulk Pd; **d**: bulk PdO. The solid lines are the experimental data, and the dotted lines are the best fit.

observed beyond the first one to the annealed material that features a very strong multipeak located at ca. 3.4 Å before phase correction, corresponding to one O shell and 2 Sn shells. Between, the other pure or Pd doped Sn/SnO_x nanocomposites samples feature a relatively strong peak located at ca. 2.8 Å before phase correction corresponding to a Sn shell. The intensity of this shell varies from one sample to the other.

As the XANES data already showed, except for the heat-treated sample, the pure or Pd doped Sn/SnO_x nanocomposites feature all very similar FT's. The first peak could be fitted for all these samples with ca. 3.2−3.3 O located at 2.071−2.074 Å from the central atom. The second peak in the FT could be fitted with ca. 0.6−1.4 Sn atoms located at 3.00−3.010 Å from the Sn scatterer atom. This shell does not belong to the tin oxide structure but corresponds to the typical Sn−Sn distance of the tin metallic phase (3.02 Å[43]). Diffraction measurements and HRTEM measurements already showed that this tin β metallic phase, corresponding to the portion of the tin that has not been oxidized is located at the core of the colloid.[9]

The remaining shells could be fitted with a combination of Sn and O atoms corresponding roughly to the cassiterite structure of SnO_2. However the intensity of these peaks is very low, and one can consider that the tin oxide phase is mainly in a disordered and/or amorphous state. This is also confirmed by the HRTEM pictures that show no trace of any crystalline structure in the layer surrounding the tin metal core but rather the presence of an amorphous phase.

The first peak of the Sn/SnO_x material coated with pvp could also be fitted with a 3.2 oxygen coordination shell but located at 2.091 Å, a larger distance than for the other samples. At the same time the second peak corresponding to the Sn−Sn bond of metallic tin has a very small intensity corresponding to 0.6 Sn atoms. The absence of any major peak located at higher *R*-values indicates as in the previous samples that these colloids have an amorphous structure.

Except for the sample that has been heat-treated at 600 °C, all Sn/SnO_x nanomaterials present an Sn coordination shell of 0.6−1.4 Sn atoms located at ca. 3.0 Å corresponding to the first coordination shell in tin β tetragonal metallic phase. The coordination numbers in EXAFS are generally determined with much less accuracy (±20%) than the bond distances but can still be used to estimate the relative amount of phases in a multiphasic material. If we consider that tin is coordinated to 4 Sn atoms located at 3.022 Å in the bulk tetragonal β metallic phase (the next 2 Sn neighbors being located further apart at 3.182 Å[43]), the relative amount of tin metallic atoms in the colloid can be estimated at 15% (0.6 × 100/4) for Sn/SnO_x particles coated with pvp polymer, ca. 25% (1 × 100/4) for the Pd doped samples, and up to 36% (1.4 × 100/4) for the pure Sn/SnO_x nanocomposite. This latter value matches exactly the ratio expected for a typical pure Sn/SnO_x of 19 nm diameter colloid[9] having an 11 nm diameter metallic core as measured on the HRTEM images. Indeed, the Sn metallic core in this case represents 27% of the total volume of the particle and 36% of the total number of tin atoms (unit cell volume of βSn =

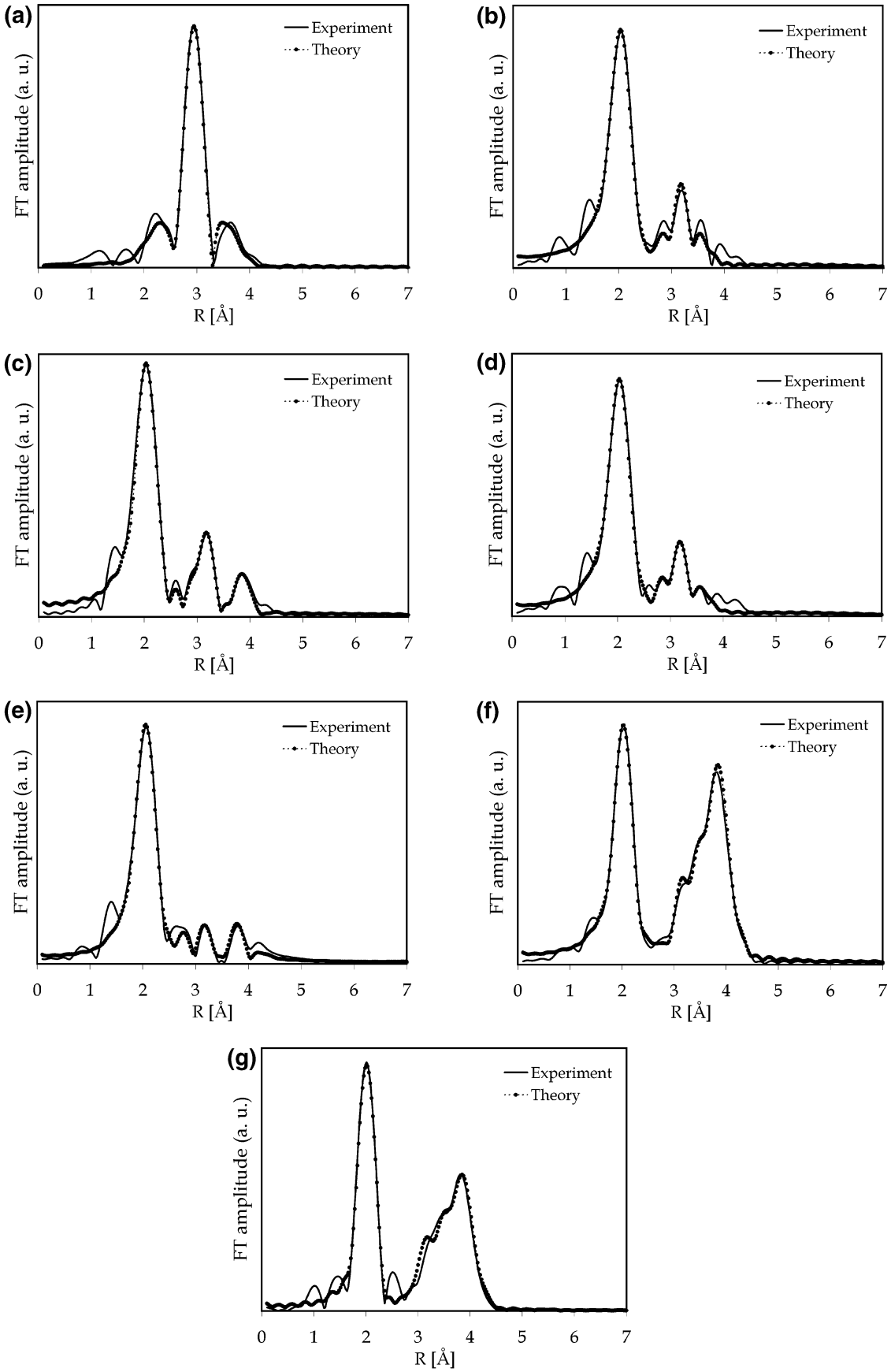

Figure 6. Fourier transforms of the Sn K-edge k^3-weighted or k^2-weighted EXAFS of the series of Sn/SnO_x nanomaterials and reference samples. **a**: bulk Sn; **b**: Sn/SnO_x; **c**: Sn/SnO_x surface-doped with Pd; **d**: Sn/SnO_x volume-doped with Pd; **e**: Sn/SnO_x coated in pvp; **f**: Sn/SnO_x annealed at 600 °C; **g**: bulk SnO_2. The solid lines are the experimental data, and the thick dotted lines are the best fit.

108.19 Å^3 with $Z = 4$ and unit cell volume of SnO_2 = 71.47 Å^3 with $Z = 2$).[43] This value of the relative part of the Sn atoms located in the tetragonal β metallic core can be used to evaluate the average oxygen coordination in the outer amorphous tin

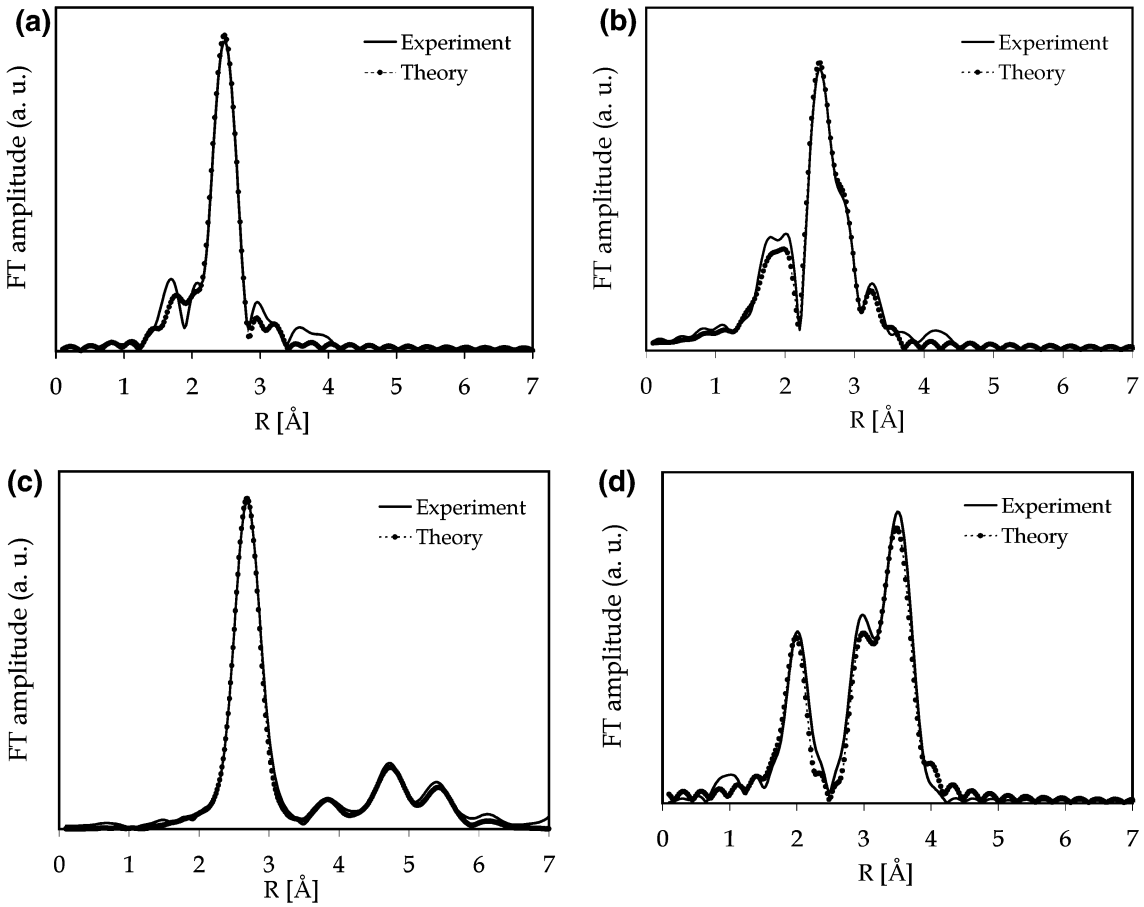

Figure 7. Fourier transforms of the Pd K-edge k^3-weighted or k^2-weighted EXAFS of Pd doped Sn/SnO_x nanomaterials and reference samples. **a**: Sn/SnO_x volume-doped with Pd; **b**: Sn/SnO_x surface-doped with Pd; **c**: bulk Pd; **d**: bulk PdO. The solid lines are the experimental data, and the thick dotted lines are the best fit.

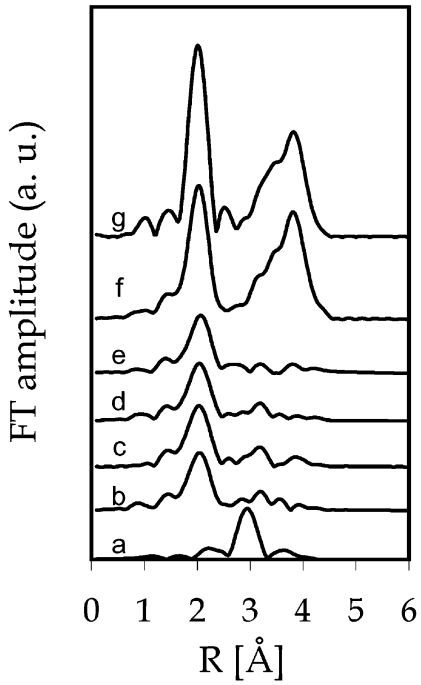

Figure 8. Fourier transforms of the Sn K-edge k^3-weighted or k^2-weighted EXAFS of the series of Sn/SnO_x nanomaterials and reference samples. **a**: bulk Sn; **b**: Sn/SnO_x; **c**: Sn/SnO_x surface-doped with Pd; **d**: Sn/SnO_x volume-doped with Pd; **e**: Sn/SnO_x coated in pvp; **f**: Sn/SnO_x annealed at 600 °C; **g**: bulk SnO_2.

oxide layer. Indeed, if only 85 to 64% of the Sn atoms are located in the oxide phase, thus the average of oxygen atoms in the first coordination shell tin oxide phase is slightly higher than 3.3 and can be estimated at 3.8 (3.2/0.85) for Sn/SnO_x in pvp, 4.4 (3.3/0.75) for both Pd-doped samples, and 5.2 (3.3/0.64) for the pure Sn/SnO_x. Tin atoms in the oxidized phase are thus 4−5-fold coordinated to oxygen with bond distances slightly larger than for the bulk SnO_2 (2.045 Å) or the thermally oxidized SnO_2 crystalline colloids (ca. 2.058 Å).

As the XANES analysis already indicated, Sn is certainly close to the +IV state as in the SnO_2 oxide phase. The presence in these material of a small fraction of SnO at the interface between the SnO_2 outer shell and the metallic Sn core has been pointed out by the diffraction and Mössbauer measurements,[9] but the inclusion of this phase in our EXAFS fitting models never led to any statistical improvement of the fit. These crystallized phases may in this case be only relatively minor phases since the EXAFS data show that the tin oxide phase is mostly in an amorphous state. Because the EXAFS technique can determine the distances in a very reliable way (±0.02 Å), another possible way to determine the oxidation state of tin atoms is to use the Sn−O distance as a guide for the extent of oxidation.[44] The average Sn−O bond distance is indeed in all the samples much closer to the tin−oxide bond distance in the SnO_2 phase (R_{SnO2} = 2.052 Å) than to the corresponding Sn−O distance in SnO (R_{SnO} = 2.21 Å).[43] If one considers that the tin coordination and the crystalline/amorphous state of the tin oxide are not influencing to a great extent the tin−oxygen bond distance, by using this simple equation $R_{SnO}(x) + R_{SnO2}(1-x) = R_{SnO2-x}$ (x being the ratio of Sn (+II) in the SnO_{2-x} phase), the ratio of Sn (+II) in tin oxide phase can be evaluated to ca. 14% in Sn/SnO_{2-x} samples with an Sn−O bond distance R_{SnO2-x}

= 2.074 Å and up to 25% for the nanocomposite coated with pvp with an average Sn−O bond distance of R_{SnO2-x} = 2.091 Å. According to this method, the average oxidation state of Sn atoms can be estimated between +3.5 (4 × (1−0.25) + 2 × 0.25) for Sn coated with pvp up to +3.7 (4 × (1−0.14) + 2 × 0.14) for the rest of the non-heat-treated samples. This evaluation shows that if some SnO phase is present in the nanocomposites, this phase, when compared to the amorphous SnO_2 phase, is always a minor phase explaining the difficulty to separate it out in the EXAFS fitting process.

No major effect of the Pd doping on the local environment of the tin atoms in this series of sample could be pointed out in our EXAFS measurements at the Sn K-edge. This can be explained by the small amount of Pd added to the tin colloids: the final molar ratio [Pd]/[Sn] is only ca. 3.09% for the surface-doped material and near ca. 7% for the volume-doped sample. However, the Fourier transforms at the Sn K-edge show for the surface-doped sample the presence of a tiny peak between the two main peaks that could be fitted with 0.1 Pd atoms located at 2.58 Å. The general fit was slightly improved when this shell was added to the EXAFS model.

In the case of the heat-treated sample, the presence of a huge multipeak beyond the first oxygen peak shows that the thermal oxidation of Sn/SnO_x nanomaterial yields indeed very crystalline nanoparticles of cassiterite SnO_2. The results of the EXAFS refinements presented in Table 1 confirmed that this SnO_2 sample has the same tetragonal cassiterite structure of bulk SnO_2. This also confirmed X-ray diffraction measurement that also pointed out the presence, in a much lower amount, of the high-pressure orthorhombic phase.[9] This orthorhombic phase that could not be pointed out in the refinement is certainly a minor phase.

In general the nanoparticles coated with pvp present a lower Sn metal content together with a higher SnO content than their uncoated counterparts. However their heat-treatment at 600 °C leads to the same SnO_2 nanoparticle size as with the uncoated Sn/SnO_x colloids. Moreover, their higher dispersion in the polymer matrix did not make any significant difference in terms of electrical properties of the oxidized material deposited on the silicon wafer when compared to the uncoated Sn/SnO_x. At the same time their deposition process was not significantly improved.

3.3.2. Pd K-Edge. The phase corrected FT's corresponding to the EXAFS measurements at the Pd K-edge of the Pd doped samples along with reference samples are presented in Figure 9. The Fourier transforms of the two Pd doped Sn/SnO_x nanomaterials are relatively different from one another. The FT of the volume-doped sample exhibits a single peak relatively sharp located before phase correction at around 2.3 Å. The FT corresponding to the surface-doped sample is composed of a much broader peak located around 2.3 Å but with a smaller satellite peak located at ca. 1.7 Å before phase correction. Moreover, the main peak features a shoulder on its right-hand side indicating the presence of 2 shells with very close distances. The intensity of the FT of the surface-doped sample is also much lower than in the case of the Pd volume-doped sample. Both FT's could be fitted with two very close shells of tin and palladium. No other peaks at higher distances could be detected indicating that the Pd phase is rather amorphous and/or that this phase is composed of very small particles. Surprisingly, no peak corresponding to an oxygen shell located at a smaller distance from the Pd could be detected showing, together with the XANES results, that Pd is not oxidized but is part of a metallic phase.

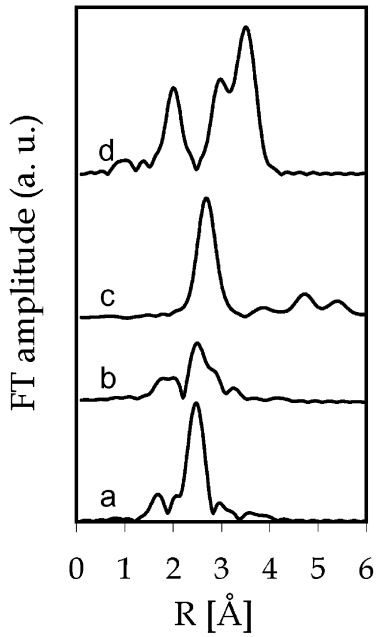

Figure 9. Fourier transforms of the Pd K-edge k^3-weighted or k^2-weighted EXAFS of Pd doped Sn/SnO_x nanomaterials and reference samples. **a**: Sn/SnO_x volume-doped with Pd; **b**: Sn/SnO_x surface-doped with Pd; **c**: bulk Pd; **d**: bulk PdO.

The results of the EXAFS refinement presented in Table 2 show that the environment around each Pd atom is composed in both samples of ca. 2.7 Sn atoms, located at a distance of 2.55 Å from the scatterer atom in the case of the volume-doped sample and at a longer distance of 2.58 Å for the surface-doped sample. The presence of tin around the palladium atoms is also confirmed by the Sn K-edge study of the surface-doped sample (see section 3.2.1). In this case a contribution of 0.1 Pd atoms located at 2.58 Å improved the fit of the data showing the consistency of the refinements conducted both at Sn and Pd K-edges. Both samples feature a second shell of palladium atoms consisting of 2.3 atoms located at 2.77 Å in the surface-doped and of only 0.5 atoms located at 2.71 Å in the volume-doped sample.

As the relative shift of the two XANES spectra already showed, the bond distances found for the volume-doped Sn/SnO_x sample are systematically shorter than for the surface-doped sample. Moreover both distances are shorter than the corresponding Sn−Sn distances (3.022 Å)[43] in bulk tin and the Pd−Pd distances (2.751 Å)[43] in bulk palladium. The formation of short tin−palladium bonds (ca. 2.63 Å) has already been observed by Choi et al.[37] in their study of tin modified alumina-supported palladium catalysts. Moreover when compared to the Pd−Sn bond distance found in a tin/palladium phase-like Pd_2Sn (Pd−Sn 2.608 Å),[43] the Pd−Sn bond distance of 2.55 Å is in the same range but still relatively smaller.

The Pd−Pd distances found in these two samples (2.71−2.77 Å) are in the same range order than those found in the palladium metallic phase. However none of these distances really matches the exact value. Even if the discrepancy observed in the bond distances (ca. 1−2%) is not so large when taken into account the relatively large esd's associated with these results, it may also indicate that the Pd atoms are located into different locations in the material and have different environments in each sample. The average Sn coordination number around the Pd atoms in the mixed Sn/Pd phase is similar and relatively low for both samples. On the contrary, the number of Pd atoms surrounding the Pd scatterer atom is different in each sample:

it is much larger for the surface doped sample. The very low value found for the volume-doped sample could be explained by a better mixing of the Sn and Pd atoms during the preparation process. Pd atoms seem to be much more dispersed into the Sn matrix in this case.

The higher total coordination number ($2.8 + 2.3 = 5.1$) found for the surface doped sample than for the volume doped sample ($2.6 + 0.5 = 3.1$) while keeping the same Sn coordination number for both samples may suggest that the major part of the Pd atoms forms a similar Sn/Pd mixed phase with low coordination Pd−Sn number in both samples, the remaining Pd atoms forming another phase with a much higher average Pd−Pd first shell coordination number. If we consider that the Pd atoms remain in a pure Pd metallic or a Pd rich phase with a 12-fold coordination, which is consistent with the Pd−Pd bond distance of 2.77 Å, then a small variation in the amount of this pure or Pd rich phase would result in a great variation of the total coordination number around Pd. In the case of the surface-doped sample the amount of the pure Pd phase could be estimated at ca. $2.3 \times 100/12 = 20\%$, while only ca. $0.5 \times 100/12 = 4\%$ of pure Pd phase would be present in the volume-doped sample.

Of course, an average view of the local structure around Sn and Pd atoms determined by the EXAFS technique does not give any direct information on the morphology of these particles. However when combined with the HRTEM images it is possible to propose two structural models.

The first one could be the presence of small pure Pd metal particles coated with Sn atoms embedded in the outer amorphous tin oxide layer. If one considers that these particles have a high ratio of Pd atoms located at the surface or more precisely at the interface Pd/Sn, then this could explain the relatively small coordination number found for the Pd−Pd shell. In this case the Sn first neighbors would correspond to an interfacial phase. This is consistent with the HRTEM pictures that show the presence of small crystallized platelets that are only present in the case of the Pd doped samples. These platelets, in larger number in the surface-doped sample, could consist of a tiny core of metallic Pd surrounded by a tin/tin oxide interface. A possible mechanism for the formation of these platelets would be that the Pd atoms are first deposited at the surface of the tin particle during the decomposition stage of the Pd precursor. They are then covered up entirely with Sn atoms that migrate around the Pd particles because of their greater affinity for oxygen than the Pd. The presence of Pd atoms located mainly at the surface of the Sn core is corroborated by the fact that the surface doping leads to nanoparticles that feature the same morphology as in the pure Sn/SnO_x nanoparticles. The surface location of the Pd atoms in the surface-doped materials is also confirmed by XPS measurements carried out together with argon surface abrasion that show clearly a decreasing Pd/Sn ratio after abrasion. The overall Pd surface ratio was then estimated at more than 70% of the Pd atoms.[45]

In the second model the Pd dopant would be present in the core metallic part of the particle in which they form a bulk alloy with Sn (with or without the presence of a pure metallic Pd phase) or even an amorphous Sn/Pd phase. This model that implies a very good mixing of the Sn and Pd atoms seems to be more consistent with the EXAFS results of the volume-doped sample. This could explain the huge increase in the size of the particle that has been observed in this case. However the HRTEM picture also shows the presence of crystalline platelets around the core of the particle. A combination of these two models could be an explanation consistent both with the EXAFS measurements and the TEM observations for the volume-doped sample. The existence of these two different systems could also explain the discrepancy in the Pd−Sn and Pd−Pd bond distances that have been observed in the EXAFS results between the two Pd-doped materials.

This first direct structural study of these Pd-doped materials has shown that they have a more complex structure than the one we would simplistically expect from the doping methods that have been used: either Pd dispersed throughout the Sn/SnO_2 particle with the codecomposition method (volume-doped) or Pd forming a surface layer on the particles with the deposition of Pd on preformed Sn/SnO_2 composites (surface-doped).

Pure and Pd doped samples have been tested for their electrical properties after a full oxidation at 600 °C in the working conditions of a gas sensor. Pure SnO_2 nanomaterial is highly sensitive to reducing gases such as CO and CH_4 with a high reproducibility and reliability level.[12] The two Pd doped samples feature very different electrical properties. If the sample doped in surface exhibits an important increase in its sensitivity to gases such as CO compared to the pure SnO_2 samples and under analogous operating mode and similar humidity level,[45,46] the volume-doped sample has shown very poor electrical properties. Indeed, the material featured always a very high resistivity, and no sensitivity to gases could be measured. Moreover the synthesis method generates some acetic acid that can attack the tin oxide phase and reduce some part of it into Sn metal. The higher Pd loading in this material, the formation of a bulk alloy Sn−Pd or a special phase that are less conductive as well as the big change in particle size are the possible explanations to account for the dramatic change of the electrical properties.

4. Conclusion

The EXAFS and XANES results showed that except for the sample annealed at 600 °C in which the tin oxide is crystallized in the cassiterite form, the major part of the tin in these Sn/SnO_x nanocomposites is forming an amorphous oxide phase in which Sn atoms are between 4- and 5-fold coordinated to oxygen atoms with an average bond distance slightly higher than in bulk cassiterite SnO_2. In very good agreement with the HRTEM results, the presence of a metallic core part estimated at 15−36% of the total amount of tin atoms with Sn−Sn bond distances close to the values found in the bulk metal could be pointed out. The Sn colloids coated with pvp were oxidized to a greater extent than the other ones and featured Sn−O bond distances longer than in the other samples. By using the Sn−oxygen bond length, the average oxidation state of Sn atoms could be estimated between +3.5 for Sn coated with pvp up to +3.7 for the rest of the nonheated samples. In general the particles coated with pvp presented a lower Sn metal content together with a higher SnO content than in their uncoated counterparts.

The Pd K-edge measurements for the two samples doped with Pd using two different methods i.e., volume and surface-doped, show that the Pd is surprisingly always in a metallic state and is surrounded by a mixture of Sn and Pd atoms located at unusually short distances. However some variations in the bond distance as well as in the number of Pd neighbors between the two samples may indicate that the Pd dopants have a different physical location in the two samples. By observing the HRTEM pictures into details, the formation by migration and rearrangement of the Pd atoms of small crystalline platelets of Pd metal embedded in the amorphous tin oxide outer layer of the particle has been suggested for the sample doped in surface. For the sample doped in volume the formation both of a bulk Sn/Pd

phase in the core part of the particle that could explain the huge increase in the particle size together with the presence of Pd platelets around it has been suggested. The electrical properties of the two fully oxidized Pd doped samples show a great difference: the sample doped in surface featuring a large increase in its gas sensitivity, while a very high resistivity with a very poor sensitivity have been measured in the sample doped in volume. This XAS study that has allowed us for the first time to directly characterize the structure of these materials has e shown that they have a more complex structure than the one that was originally assumed. This investigation by pointing out more specifically the role of the doping element in the two doping methods should lead to significant improvements in the optimization of the preparation method of these nanocomposites.

Acknowledgment. For financial support we thank the EU TMR program contract number FMRX-CT98-0177. Access to the synchrotron facilities at the SRS was arranged through the general support of the EPSRC for the use of central facilities. We wish to acknowledge the assistance and advice of Dr. Fred Mosselmans (SRS 9.2) during the experimental measurements. We also wish to acknowledge the use of the EPSRC's Chemical Database Service at Daresbury.

References and Notes

(1) Micocci, G.; Serra, A.; Siciliano, P.; Tepore, A.; Ali-Abid, Z. *Vacuum* **1996**, *47*, 1175.
(2) Demarne, V.; Grisel, A. *Sens. Actuators, B* **1993**, *15*−*16*, 63.
(3) Liu, Y.; Zhu, W.; Tan, O. K.; Yao, X.; Shen, Y. *Vacuum* **1996**, *7*, 279.
(4) Yamazoe, N. *Sens. Actuators, B* **1991**, *5*, 7.
(5) Ocana, M.; Matijevic, E. *J. Mater. Res.* **1990**, *5*, 1083.
(6) Dieguez, A.; Romano-Rodriguez, A.; Morante, J. R.; Weimar, U.; Schweizer-Berberich, M.; Goepel, W. *Solid State Phenom*. **1996**, *51*−*52*, 441.
(7) Ivanovskaya, M. I.; Bogdanov, P. A.; Orlik, D. R.; Gurlo, A. C.; Romanovskaya, V. V. *Thin Solid Films* **1997**, *296*, 41.
(8) Nayral, C.; Ould-Ely, T.; Maisonnat, A.; Chaudret, B.; Fau, P.; Lescouzeres, L.; Peyre-Lavigne, A. *Adv. Mater.* **1999**, *11*, 61.
(9) Nayral, C.; Viala, E.; Fau, P.; Senocq, F.; Jumas, J. C.; Maisonnat, A.; Chaudret, B. *Chem. Eur. J.* **2000**, *6*, 4082.
(10) Nayral, C.; Viala, E.; Colliere, V.; Fau, P.; Senocq, F.; Maisonnat, A.; Chaudret, B. *Appl. Surf. Sci.* **2000**, *164*, 219.
(11) Fau, P.; Nayral, C.; Chaudret, B.; Maisonnat, A. *Motorola*, European patent N°98400246.9-2104.
(12) Fau, P.; Sauvan, M.; Trautweiler, S.; Nayral, C.; Erades, L.; Maisonnat, A.; Chaudret, B. *Sens. Actuators, B* **2001**, *78*, 83.
(13) Norris, J. O. W. In *The Role of Precious Metal Catalysts*; Adam Hilger: Bristol, 1987.
(14) Schweizer-Berberich, M.; Zheng, J. G.; Weimar, U.; Goepel, W.; Barsan, N.; Pentia, E.; Tomescu, A. *Sens. Actuators, B* **1996**, *B31*, 71.
(15) Yamazoe, N. *Sens. Actuators, B* **1991**, *B5*, 7.
(16) Shimizu, Y.; Egashira, M. *MRS Bull.* **1999**, *24*, 18.
(17) Matsushima, S.; Teraoka, Y.; Miura, N.; Yamazoe, N. *Jpn. J. Appl. Phys*. **1988**, *27*, 1798.
(18) Matsushima, S.; Tamaki, J.; Miura, N.; Yamazoe, N. *Chem. Lett.* **1989**, 1651.
(19) Labeau, M.; Gautheron, B.; Cellier, F.; Vallet-Regi, M.; Garcia, E.; Gonzalez Calbet, J. M. *J. Solid State Chem.* **1993**, *102*, 434.
(20) Dieguez, A.; Vila, A.; Cabot, A.; Romano Rodriguez, A.; Morante, J. R.; Kappler, J.; Barsan, N.; Weimar, U.; Gopel, W. *Sens. Actuators, B* **2000**, *68*, 94.
(21) Wagner, C. D.; Naumkin, A. V.; Kraut-Vass, A.; Allison, J. W.; Powell, C. J.; Rumble, J. R., Jr. X-ray Photolectron Spectroscopy Database (NIST Standard Reference Database 20, Web version 3.3).
(22) Brito, G. E. S.; Ribeiro, S. J. L.; Briois, V.; Dexpert-Ghys, J.; Santilli, C. V.; Pulcinelli, S. H. *J. Sol-Gel Sci. Technol.* **1997**, *8*, 261.
(23) Brito, G. E. S.; Briois, V.; Pulcinelli, S. H.; Santilli, C. V. *J. Sol-Gel Sci. Technol.* **1997**, *8*, 269.
(24) Briois, V.; Santilli, C. V.; Pulcinelli, S. H.; Brito, G. E. S. *J. Non-Cryst. Solids* **1995**, *191*, 17.
(25) Davis, S. R.; Chadwick, A. V.; Wright, J. D. *J. Phys. Chem. B* **1997**, *101*, 9908.
(26) Davis, S. R.; Chadwick, A. V.; Wright, J. D. *J. Mater. Chem.* **1998**, *8*, 2065.
(27) Jimenez, V. M.; Caballero, A.; Fernandez, A.; Espinos, J. P.; Ocana, M.; Gonzalez-Elipe, A. R. *Solid State Ionics* **1999**, *116*, 117.
(28) Santilli, C. V.; Pulcinelli, S. H.; Brito, G. E. S.; Briois, V. *J. Phys. Chem. B* **1999**, *103*, 2660.
(29) Serrini, P.; Briois, V.; Horillo, M. C.; Traverse, A.; Manes, L. *Thin Solid Films* **1997**, *304*, 113.
(30) Gaidi, M.; Labeau, M.; Chenevier, B.; Hazemann, J. L. *Sens. Actuators, B* **1998**, *48*, 277.
(31) Rockenberger, J.; zum Felde, U.; Tischer, M.; Tröger, L.; Haase, M.; Weller, H. J. *Chem. Phys.* **2000**, *112*, 4296.
(32) Morris, L.; Williams, D. E.; Kaltsoyannis, N.; Tocher, A. *Phys. Chem. Chem. Phys.* **2001**, *3*, 132.
(33) Briois, V.; Pulcinelli, S. H.; Santilli, C. V. *J. Mater. Sci. Lett.* **2001**, *20*, 555.
(34) Lopez-Navarrete, E.; Caballero, A.; Orera, V. M.; Lazaro, F. J.; Ocana, M. *Acta Mater.* **2003**, *51*, 2371.
(35) Harrison, P. G.; Lloyd, N. C.; Daniell, W.; Bailey, C.; Azelee, W. *Chem. Mater.* **1999**, *11*, 896.
(36) Revel, R.; Bazin, D.; Bouchet-Fabre, B.; Seigneurin, A.; Kihn, Y. *J. Phys. IV* **2002**, *12*, 309.
(37) Choi, S. H.; Lee, J. S. *J. Catal.* **2000**, *193*, 176.
(38) Lecante, P.; Kihn Y.; Dexpert, H.; Gaidi, M.; Holderer, O.; Fuchs, G.; Bertucci, M. *J. Phys. IV* **2002**, *12*, 481.
(39) Moseley, P. T.; Maitlis, P. J. *Chem. Soc., Chem. Commun.* **1971**, 982.
(40) Binsted, N.; Campbell, J. W.; Gurman, S. J.; Stephenson, P. C. *EXAFS Analysis Programs*; Daresbury Laboratory: Warrington 1991.
(41) Bianconi, A. In *X-ray Absorption, Principles, Applications, Techniques of EXAFS, SEXAFS and XANES*; Koningsberger, D. C., Prins. R., Eds.; Wiley: New York; 1988; Chapter 11.
(42) Pandey, S. K.; Chetal, A. R. *Phys. Stat. Sol.* **1992**, *170*, 631.
(43) The United Kingdom Chemical Database Service. Fletcher, D. A.; McMeeking, R. F.; Parkin, D. *J. Chem. Inf. Comput. Sci.* **1996**, *36*, 746.
(44) Barett, P. A.; Sankar, G.; Catlow, R. A.; Thomas, J. M. *J. Phys. Chem.* **1996**, *100*, 8982.
(45) Erades, L.; Nayral, C.; Soulantica, K.; Maisonnat, A.; Chaudret, B.; Grandjean, D.; Benfield, R. E. Submitted for publication.
(46) Menini, P.; Parret, F.; Guerrero, M.; Martinez, A.; Soulantica, K.; Erades, L.; Maisonnat, A.; Chaudret, B. *Sens. Actuators, B* In press.